


Graph Regularized NMF with $\ell_{2,0}$ -norm for Unsupervised Feature Learning

Zhen Wang and Wenwen Min*

Abstract—Nonnegative Matrix Factorization (NMF) is a widely applied technique in the fields of machine learning and data mining. Graph Regularized Non-negative Matrix Factorization (GNMF) is an extension of NMF that incorporates graph regularization constraints. GNMF has demonstrated exceptional performance in clustering and dimensionality reduction, effectively discovering inherent low-dimensional structures embedded within high-dimensional spaces. However, the sensitivity of GNMF to noise limits its stability and robustness in practical applications. In order to enhance feature sparsity and mitigate the impact of noise while mining row sparsity patterns in the data for effective feature selection, we introduce the $\ell_{2,0}$ -norm constraint as the sparsity constraints for GNMF. We propose an unsupervised feature learning framework based on GNMF_ $\ell_{2,0}$ and devise an algorithm based on PALM and its accelerated version to address this problem. Additionally, we establish the convergence of the proposed algorithms and validate the efficacy and superiority of our approach through experiments conducted on both simulated and real image data.

Index Terms—graph learning, NMF, feature selection, $\ell_{2,0}$ -norm, non-convex optimization



1 INTRODUCTION

NONNEGATIVE matrix factorization (NMF) is a widely used technique in the fields of machine learning [1–4] and data mining [5–10]. It decomposes a nonnegative data matrix into the product of two nonnegative matrices, where one matrix represents the latent feature representation of the samples and the other matrix represents the weights of the features. NMF’s advantage lies in its ability to discover latent structures and patterns in the data, making it applicable in tasks such as clustering, dimensionality reduction, and feature learning. However, traditional NMF methods do not consider the local and global structural information of the data, leading to suboptimal performance on complex datasets.

To overcome this limitation, Graph Regularized Nonnegative Matrix Factorization (GNMF) has been introduced [11–15]. GNMF incorporates the prior information of the graph structure to assist in feature learning and effectively explore the latent clustering structure in the data. In GNMF, the similarity between samples is mapped onto a graph and combined with the nonnegative matrix factorization approach for feature learning. This allows GNMF to better preserve the local neighborhood and global consistency of the samples, thereby improving the performance of clustering and dimensionality reduction. However, traditional GNMF methods exhibit some sensitivity when dealing with noisy data, limiting their stability and robustness in practical applications, sparse constraints need to be introduced [16, 17].

Sparse constraints help improve the uniqueness of decomposition and enhance locally based representation, and in practice, they are almost necessary. The introduction of ℓ_2 and ℓ_1 norms serves to mitigate the impact of noise and outliers [16, 18], and the $\ell_{2,1}$ -norm can be utilized to quantify the error in matrix

factorization, thereby enhancing robustness [17, 19]. However, these sparsity constraints mentioned above do not pay attention to the row sparsity pattern in the data matrix \mathbf{X} , making these sparse methods unable to select important features in the data matrix for cluster analysis.

To enhance the sparsity of GNMF and mitigate the influence of noise, this paper introduces the $\ell_{2,0}$ -norm constraint as an improvement. The $\ell_{2,0}$ -norm constraint is a regularization method based on the $\ell_{2,0}$ -norm, which effectively encourages the reduction of less significant features in the feature matrix, pushing them toward zero and thus achieving a sparse representation of features [20–23]. By incorporating the $\ell_{2,0}$ -norm constraint, we can further enhance the performance of feature learning and improve the robustness against noisy data. The workflow of the GNMF_ $\ell_{2,0}$ model is shown in Figure 1. It applies graph regularization and $\ell_{2,0}$ -norm constraint on the basis of NMF, allowing the model to better mine and utilize the geometric information of the data space and extract important features. However, due to the non-convex and non-smooth nature of the $\ell_{2,0}$ -norm constraint in the model, common convex optimization methods cannot solve this optimization problem.

To address this issue, this paper proposes an unsupervised feature learning framework based on GNMF_ $\ell_{2,0}$ and designs the corresponding PALM algorithm and its accelerated version to tackle this problem. The PALM algorithm is an alternating linear minimization method proposed for a class of non-convex and non-smooth problems that satisfy the Kurdyka-Łojasiewicz (KŁ) property [24, 25]. It optimizes the objective function by iteratively updating the characteristic matrix and weight matrix. Fortunately, our GNMF_ $\ell_{2,0}$ framework satisfies the KŁ property, so the PALM method can be used to solve our problem.

In addition, there are other non-convex optimization algorithms, such as iPALM [26] and BPL [27]. iPALM represents the inertial version of the PALM algorithm, while BPL is a non-convex optimization algorithm with global convergence based on block-coordinate updates. Both of the above methods add an extrapolation step to speed up the algorithm, inspired by these

• Zhen Wang and Wenwen Min is with the School of Information Science and Engineering, Yunnan University, Kunming 650091, Yunnan, China, China. E-mail: minwenwen@ynu.edu.cn.

Manuscript received XX, 2023; revised XX, 2023.
(Corresponding authors: Wenwen Min)

advancements, we develop a new accPALM acceleration algorithm based on the PALM method, which accelerates the convergence of the algorithm by introducing extrapolation during the iterative process and the degree of acceleration can be controlled by adjusting the extrapolation parameters. Additionally, we provide convergence analysis to guarantee the convergence and stability of the algorithm during the optimization process. We show that both the PALM and accPALM algorithms can converge to a critical point when solving the GNMF- $\ell_{2,0}$ model.

Our main contributions are summarized as follows:

- 1) Addressing the sensitivity of GNMF to noisy data, we introduce the $\ell_{2,0}$ -norm constraint to enhance the sparsity of features, propose an unsupervised feature learning framework based on GNMF- $\ell_{2,0}$.
- 2) We propose a novel algorithm based on PALM and its accelerated version to solve the proposed GNMF- $\ell_{2,0}$ model. Convergence analysis is provided to ensure the effectiveness and stability of the algorithm.
- 3) We validate the effectiveness of the proposed method through experiments on both simulated and real-world datasets, compare it with other benchmark methods, and discuss the sparsity of features.

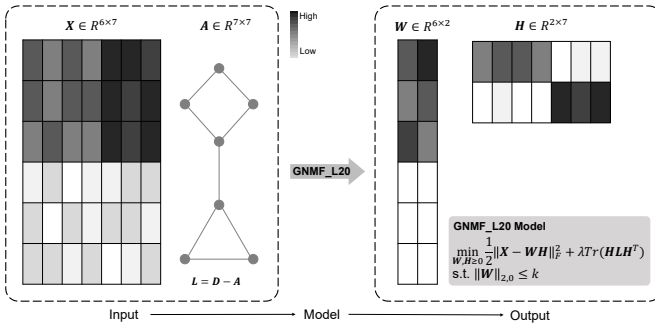


Figure 1. GNMF- $\ell_{2,0}$ matrix factorization and clustering process. The input of GNMF- $\ell_{2,0}$ is a two-dimensional matrix \mathbf{X} . The adjacency matrix \mathbf{A} is constructed through the data matrix \mathbf{X} to represent the correlation between data points. GNMF- $\ell_{2,0}$ decomposes \mathbf{X} into two low-dimensional matrices, namely the basis matrix \mathbf{W} and the coefficient matrix \mathbf{H} . The \mathbf{H} matrix is useful for sample clustering and visualization in low-dimensional space, while the $\hat{\mathbf{X}} = \mathbf{WH}$ can be used for downstream analysis.

2 RELATED WORK

In this section, we present the model frameworks of NMF and GNMF along with relevant symbols and definitions.

2.1 NMF

NMF aims to decompose a non-negative data matrix \mathbf{X} into the product of two non-negative matrices, \mathbf{W} and \mathbf{H} , i.e., $\mathbf{X} \approx \mathbf{WH}$. Here, \mathbf{W} represents the matrix of latent feature representations of the samples, and \mathbf{H} represents the matrix of weights for the features. The loss function of NMF is based on the reconstruction error using the Euclidean distance. The standard NMF algorithm employs the Frobenius norm to quantify the dissimilarity between the original matrix \mathbf{X} and the reconstructed matrix \mathbf{WH} . Specifically, the Frobenius norm of the matrix \mathbf{X} , denoted as $\|\mathbf{X}\|_F$, is defined as the square root of the sum of

squared elements of \mathbf{X} , represented as $\|\mathbf{X}\|_F^2 = \sum_{ij} \mathbf{X}_{ij}^2$. Given a data matrix $\mathbf{X} = [x_{ij}] \in \mathbb{R}_+^{p \times n}$ with p features and n samples, the NMF model [28] can be expressed as:

$$\begin{aligned} \min_{\mathbf{W}, \mathbf{H}} \|\mathbf{X} - \mathbf{WH}\|_F^2 \\ \text{s.t. } \mathbf{W} \in \mathbb{R}_+^{p \times r}, \mathbf{H} \in \mathbb{R}_+^{r \times n}. \end{aligned} \quad (1)$$

2.2 GNMF

NMF attempts to find a set of basis vectors to approximate the original data. The expectation is that these basis vectors can accurately capture the intrinsic Riemannian structure inherent in the data. To observe the local geometric structure of the original data, Cai et al. proposed GNMF [11], which incorporates a k-nearest neighbor graph \mathbf{A} , known as the adjacency matrix. For a k-nearest neighbor graph, each sample selects its k nearest samples as its neighbors based on distances or similarities, and edges are placed between these two elements.

In some cases, weights can be assigned to the elements of the adjacency matrix to indicate the strength of connections or similarities between nodes. The definition of weights can be based on distance, similarity measures, or other domain knowledge. Three of the most frequently employed are as follows [11, 29]:

- 1) **0-1 weight:** If two vertices, \mathbf{x}_j and \mathbf{x}_l , are interconnected, their weight a_{jl} is assigned a value of 1. Conversely, if they are not connected, a_{jl} is set to 0.

$$a_{jl} = \begin{cases} 1 & \text{if } \mathbf{x}_j \text{ and } \mathbf{x}_l \text{ are connected,} \\ 0 & \text{otherwise.} \end{cases} \quad (2)$$

- 2) **Gaussian kernel weight:** The Gaussian kernel function is a distance-based function, assigning higher weights to data points that are closer in distance and lower weights to data points that are farther away.

$$a_{jl} = \begin{cases} e^{-\frac{\|\mathbf{x}_l - \mathbf{x}_j\|^2}{2\sigma^2}} & \text{if } \mathbf{x}_j \text{ and } \mathbf{x}_l \text{ are connected,} \\ 0 & \text{otherwise.} \end{cases} \quad (3)$$

- 3) **Dot-Product Weighting:** Dot product weighting entails evaluating the dot product of two vectors to gauge their similarity or degree of correlation. This similarity measure is then harnessed to allocate weights to the vectors. It's important to underscore that in scenarios where vector normalization is implemented, the dot product aligns with the cosine similarity between the vectors.

$$a_{jl} = \begin{cases} \mathbf{x}_j^T \mathbf{x}_l & \text{if } \mathbf{x}_j \text{ and } \mathbf{x}_l \text{ are connected,} \\ 0 & \text{otherwise.} \end{cases} \quad (4)$$

Unless otherwise specified, Gaussian kernel weighting is adopted in this study as the method for assessing similarities.

In the study of manifold learning, given an adjacency matrix $\mathbf{A} \in \mathbb{R}^{n \times n}$, the smoothness of the original data in the low-dimensional representation is expressed as:

$$\mathcal{R} = \sum_{j,l=1}^n \|\mathbf{h}_j - \mathbf{h}_l\|^2 a_{jl}, \quad (5)$$

where a_{jl} represents the number in the j -th row and l -th column of the adjacency matrix \mathbf{A} , denote h_j as the j -th column of \mathbf{H} , $h_j = [h_{1j}, \dots, h_{rj}]^T$. The Eq.(5) can be simplified as:

$$\begin{aligned} \mathcal{R} &= \sum_{j,l=1}^n \|\mathbf{h}_j - \mathbf{h}_l\|^2 a_{jl} \\ &= \sum_{j=1}^n \mathbf{h}_j^T \mathbf{h}_j \mathbf{d}_{jj} - \sum_{j,l=1}^n \mathbf{h}_j^T \mathbf{h}_l a_{jl} \\ &= \text{Tr}(\mathbf{H}\mathbf{D}\mathbf{H}^T) - \text{Tr}(\mathbf{H}\mathbf{A}\mathbf{H}^T) \\ &= \text{Tr}(\mathbf{H}\mathbf{L}\mathbf{H}^T), \end{aligned} \quad (6)$$

where the $\text{Tr}(\cdot)$ represents the trace of a matrix, and \mathbf{D} is a diagonal matrix with entries representing the column sums of \mathbf{A} (or row sums, since \mathbf{A} is symmetric), denoted as $\mathbf{d}_{jj} = \sum_l a_{jl}$. The matrix $\mathbf{L} = \mathbf{D} - \mathbf{A}$ is referred to as the graph Laplacian, which captures the graph structure of the data.

By incorporating the graph regularization penalty term into the NMF framework, the problem of GNMF can be formulated as follows:

$$\begin{aligned} \min_{\mathbf{W}, \mathbf{H}} \quad & \|\mathbf{X} - \mathbf{W}\mathbf{H}\|_F^2 + \lambda \text{Tr}(\mathbf{H}\mathbf{L}\mathbf{H}^T) \\ \text{s.t.} \quad & \mathbf{W} \in \mathbb{R}_+^{p \times r}, \mathbf{H} \in \mathbb{R}_+^{r \times n}. \end{aligned} \quad (7)$$

GNMF introduces graph regularization constraint on the basis of NMF, which enhances the performance of feature learning by mapping the similarities between samples onto the graph.

In summary, the GNMF framework combines the capability of feature learning with the graph regularization constraint, allowing for better discovery of the underlying structure and patterns in the data. However, traditional GNMF methods are sensitive to noisy data. To enhance sparsity and mitigate the impact of noise, we introduce the $\ell_{2,0}$ -norm constraint, which will be discussed in detail in the following sections.

3 PROPOSED FRAMEWORK

In this section, a detailed introduction is provided for the formulation of the GNMF- ℓ_{20} objective function, the PALM algorithm and its accelerated version, as well as the convergence analysis.

3.1 GNMF- ℓ_{20}

First, we define a function $I(x)$ as follows:

$$I(x) = \begin{cases} 1 & \text{if } x \neq 0, \\ 0 & \text{if } x = 0. \end{cases}$$

For a given matrix $\mathbf{W} \in \mathbb{R}^{p \times r}$, the $\ell_{2,0}$ -norm represents the number of non-zero rows. Specifically, the $\ell_{2,0}$ -norm of \mathbf{W} is described as follows:

$$\|\mathbf{W}\|_{2,0} = \sum_{i=1}^p I(\|w^i\|), \quad (8)$$

where w^i denote the i -th row of \mathbf{W} , $\|\cdot\|$ is the l_2 -norm and $\|x\| = \sum x_i^2$.

To integrate feature selection and graph regularization constraints in the NMF model, and enhance the sparsity and stability of the model, we introduce a row-sparse GNMF model with $\ell_{2,0}$ -norm constraint (GNMF- ℓ_{20}):

$$\begin{aligned} \min_{\mathbf{W}, \mathbf{H}} \quad & \frac{1}{2} \|\mathbf{X} - \mathbf{W}\mathbf{H}\|_F^2 + \lambda \text{Tr}(\mathbf{H}\mathbf{L}\mathbf{H}^T) \\ \text{s.t.} \quad & \mathbf{W} \in \mathbb{R}_+^{p \times r}, \|\mathbf{W}\|_{2,0} \leq k, \mathbf{H} \in \mathbb{R}_+^{r \times n}. \end{aligned} \quad (9)$$

By imposing the constraint $\|\mathbf{W}\|_{2,0} \leq k$, we encourage sparsity in the rows of \mathbf{W} and select the most important k features.

3.2 Proposed algorithm based on PALM

PALM [24] (Proximal Alternating Linearized Minimization) algorithm is a widely used optimization algorithm for solving a class of non-convex and non-smooth minimization problems. The key idea of the PALM algorithm is to decompose the original problem into two subproblems and iteratively solve them alternatively.

In order to apply the PALM algorithm to solve our model, we reformulate the objective function of GNMF- ℓ_{20} (9) as follows:

$$\min_{\mathbf{W}, \mathbf{H}} F(\mathbf{W}, \mathbf{H}) + \delta_{\mathbf{W} \in \{\mathbb{R}_+^{p \times r}, \|\mathbf{W}\|_{2,0} \leq k\}} + \delta_{\mathbf{H} \in \{\mathbb{R}_+^{r \times n}\}}, \quad (10)$$

where $F(\mathbf{W}, \mathbf{H}) = \frac{1}{2} \|\mathbf{X} - \mathbf{W}\mathbf{H}\|_F^2 + \lambda \text{Tr}(\mathbf{H}\mathbf{L}\mathbf{H}^T)$, and the indicator function $\delta_{\mathbf{H} \in \{\mathbb{R}_+^{r \times n}\}}$ is defined as follows:

$$\delta_{\mathbf{H} \in \{\mathbb{R}_+^{r \times n}\}} = \begin{cases} 0 & \text{if } \mathbf{H} \in \{\mathbb{R}_+^{r \times n}\}, \\ +\infty & \text{otherwise,} \end{cases}$$

the indicator function $\delta_{\mathbf{W} \in \{\mathbb{R}_+^{p \times r}, \|\mathbf{W}\|_{2,0} \leq k\}}$ has a similar definition. Furthermore, let:

$$f(\mathbf{W}) = \delta_{\mathbf{W} \in \{\mathbb{R}_+^{p \times r}, \|\mathbf{W}\|_{2,0} \leq k\}},$$

$$g(\mathbf{H}) = \delta_{\mathbf{H} \in \{\mathbb{R}_+^{r \times n}\}}.$$

The objective function of GNMF- ℓ_{20} (9) can be transformed as follows:

$$\min_{\mathbf{W}, \mathbf{H}} J(\mathbf{W}, \mathbf{H}) := F(\mathbf{W}, \mathbf{H}) + f(\mathbf{W}) + g(\mathbf{H}). \quad (11)$$

Before giving the formal algorithm framework, we need to demonstrate that the PALM algorithm can be applied to our GNMF- ℓ_{20} model. Theorem 1 in [30] shows that $F(\mathbf{W}, \mathbf{H})$, $f(\mathbf{W})$ and $g(\mathbf{H})$ are semi-algebraic functions, therefore, $J(\mathbf{W}, \mathbf{H})$ is also a semi-algebraic function. Furthermore, it is obvious that $J(\mathbf{W}, \mathbf{H})$ is a proper and lower semicontinuous function. Combined with Theorem 3 of [24], we can know that $J(\mathbf{W}, \mathbf{H})$ satisfies the KL property, which means that the PALM algorithm can be used to solve our GNMF- ℓ_{20} model.

We first define the proximal map here, let $\sigma : \mathbb{R}^d \rightarrow (-\infty, \infty]$ be a proper and lower semicontinuous function. Given $x \in \mathbb{R}^d$ and $t > 0$, the proximal map associated to σ is defined by:

$$\text{prox}_t^\sigma(x) := \text{argmin} \left\{ \sigma(u) + \frac{t}{2} \|u - x\|^2 : u \in \mathbb{R}^d \right\}. \quad (12)$$

Further, when σ is the indicator function of a nonempty and closed set X as $\mathbb{R}_+^{r \times n}$, the proximal map (12) reduces to the projection operator onto X , defined by:

$$P_X(v) := \text{argmin} \{ \|u - v\| : u \in X \}. \quad (13)$$

A fundamental algorithmic framework for solving Eq. (11) is presented in Algorithm 1. Based on Algorithm 1, we also develop an accelerated proximal gradient method with adaptive momentum in Algorithm 2 to accelerate the convergence of the objective function. This algorithm combines the proximal gradient method and the extrapolation method to ensure that the objective function is monotonic and non-increasing. In each step, we compare the function value of J after the projected gradient descent of the extrapolated point and the original point respectively, and select a method with a smaller function value for the next iteration, and

Algorithm 1 PALM algorithm for solving Eq. (11)

Require: $\mathbf{X} \in \mathbb{R}^{p \times n}$.

Ensure: $\mathbf{W} \in \mathbb{R}^{p \times r}$ and $\mathbf{H} \in \mathbb{R}^{r \times n}$.

- 1: Initialization: $(\mathbf{W}^0, \mathbf{H}^0), k = 0$.
 - 2: **While** until convergence or stopping criterion **do**
 - 3: Compute c_k
 - 4: $\mathbf{W}^{k+1} \in \text{prox}_{c_k}^f \left(\mathbf{W}^k - \frac{1}{c_k} \nabla_{\mathbf{W}} F(\mathbf{W}^k, \mathbf{H}^k) \right)$
 - 5: Compute d_k
 - 6: $\mathbf{H}^{k+1} \in \text{prox}_{d_k}^g \left(\mathbf{H}^k - \frac{1}{d_k} \nabla_{\mathbf{H}} F(\mathbf{W}^{k+1}, \mathbf{H}^k) \right)$
 - 7: $k \leftarrow k + 1$
 - 8: **return** \mathbf{W}^k and \mathbf{H}^k
-

Algorithm 2 accPALM algorithm with adaptive momentum

Require: $\mathbf{X} \in \mathbb{R}^{p \times n}$.

Ensure: $\mathbf{W} \in \mathbb{R}^{p \times r}$ and $\mathbf{H} \in \mathbb{R}^{r \times n}$.

- 1: Initialization: $(\mathbf{W}^{-1}, \mathbf{H}^{-1}) = (\mathbf{W}^0, \mathbf{H}^0), \beta_0 \in [0, \beta_{\max}], \beta_{\max} < 1, k = 0, t > 1$.
 - 2: **repeat**
 - 3: $\widetilde{\mathbf{W}}^k = \mathbf{W}^k + \beta_k(\mathbf{W}^k - \mathbf{W}^{k-1})$
 - 4: compute c_k
 - 5: $\widetilde{\mathbf{W}}^{k+1} \in \text{prox}_{c_k}^f \left(\widetilde{\mathbf{W}}^k - \frac{1}{c_k} \nabla_{\mathbf{W}} F(\widetilde{\mathbf{W}}^k, \mathbf{H}^k) \right)$
 - 6: $\widetilde{\mathbf{H}}^k = \mathbf{H}^k + \beta_k(\mathbf{H}^k - \mathbf{H}^{k-1})$
 - 7: compute d_k
 - 8: $\widetilde{\mathbf{H}}^{k+1} \in \text{prox}_{d_k}^g \left(\widetilde{\mathbf{H}}^k - \frac{1}{d_k} \nabla_{\mathbf{H}} F(\widetilde{\mathbf{W}}^{k+1}, \widetilde{\mathbf{H}}^k) \right)$
 - 9: **if** $F(\widetilde{\mathbf{W}}^{k+1}, \widetilde{\mathbf{H}}^{k+1}) \leq F(\mathbf{W}^k, \mathbf{H}^k) - \rho_0 \|(\mathbf{W}^{k+1} - \widetilde{\mathbf{W}}^k, \mathbf{H}^{k+1} - \widetilde{\mathbf{H}}^k)\|^2$ **then**
 - 10: Update $\beta_{k+1} = \min(t * \beta_k, \beta_{\max})$
 - 11: $\mathbf{W}^{k+1} = \widetilde{\mathbf{W}}^{k+1}, \mathbf{H}^{k+1} = \widetilde{\mathbf{H}}^{k+1}$
 - 12: **else**
 - 13: $\mathbf{W}^{k+1} \in \text{prox}_{c_k}^g \left(\mathbf{W}^k - \frac{1}{c_k} \nabla_{\mathbf{W}} F(\mathbf{W}^k, \mathbf{H}^k) \right)$
 - 14: $\mathbf{H}^{k+1} \in \text{prox}_{c_k}^g \left(\mathbf{H}^k - \frac{1}{c_k} \nabla_{\mathbf{H}} F(\mathbf{W}^{k+1}, \mathbf{H}^k) \right)$
 - 15: Update $\beta_{k+1} = \beta_k / t$
 - 16: **end if**
 - 17: set $k = k + 1$
 - 18: **until** $\frac{\|(\mathbf{W}_k, \mathbf{H}_k) - (\mathbf{W}_{k-1}, \mathbf{H}_{k-1})\|}{\|(\mathbf{W}_{k-1}, \mathbf{H}_{k-1})\|} < \epsilon$.
 - 19: **return** $\mathbf{W} := \mathbf{W}_k$ and $\mathbf{H} := \mathbf{H}_k$
-

the extrapolation parameter β change dynamically as the iteration proceeds.

Next, we will compute the partial derivatives of F with respect to \mathbf{W} and \mathbf{H} :

$$\nabla_{\mathbf{H}} F = \mathbf{W}^T \mathbf{W} \mathbf{H} - \mathbf{W}^T \mathbf{X} + 2\lambda \mathbf{H} \mathbf{L}, \quad (14a)$$

$$\nabla_{\mathbf{W}} F = \mathbf{W} \mathbf{H} \mathbf{H}^T - \mathbf{X} \mathbf{H}^T. \quad (14b)$$

The Hessian matrices of F on \mathbf{W} and \mathbf{H} are as follows:

$$\nabla_{\mathbf{H}}^2 F = \mathbf{I}_n \otimes (\mathbf{W}^T \mathbf{W}) + (2\lambda \mathbf{L}^T) \otimes \mathbf{I}_r, \quad (15a)$$

$$\nabla_{\mathbf{W}}^2 F = (\mathbf{H} \mathbf{H}^T) \otimes \mathbf{I}_p, \quad (15b)$$

where $\mathbf{I}_p \in \mathbb{R}^{p \times p}$ is an identity matrix, and \otimes is the Kronecker product. We have known that $\nabla_{\mathbf{W}} F$ and $\nabla_{\mathbf{H}} F$ are Lipschitz continuous [31], so the Lipschitz constant of $\nabla_{\mathbf{W}} F$ is the largest singular value of $\nabla_{\mathbf{W}}^2 F$, i.e., $L_{\mathbf{W}} = \|\mathbf{H} \mathbf{H}^T\|_2$. Similarly, we can obtain that $L_{\mathbf{H}} = \|\mathbf{W}^T \mathbf{W}\|_2 + \|2\lambda \mathbf{L}^T\|_2$. The step size c_k and d_k in Algorithms 1 and 2 need to meet $c_k \geq L_{\mathbf{W}}$ and $d_k \geq L_{\mathbf{H}}$, and we can simply set $c_k = L_{\mathbf{W}}$ and $d_k = L_{\mathbf{H}}$.

Since both non-coupling terms in the equation are indicator functions, the proximal mapping operations in the iterative steps of \mathbf{W} and \mathbf{H} can be simplified to the following proximal projections:

$$P_f(\overline{\mathbf{W}}) := \operatorname{argmin} \left\{ \|\mathbf{W} - \overline{\mathbf{W}}\| : \mathbf{W} \in \{\mathbb{R}_+^{p \times r}, \|\mathbf{W}\|_{2,0} \leq k\} \right\}, \quad (16)$$

$$P_g(\overline{\mathbf{H}}) := \operatorname{argmin} \left\{ \|\mathbf{H} - \overline{\mathbf{H}}\| : \mathbf{H} \in \{\mathbb{R}_+^{r \times n}\} \right\}, \quad (17)$$

where $\overline{\mathbf{W}} := \mathbf{W}^k - \frac{1}{c_k} \nabla_{\mathbf{W}} F(\mathbf{W}^k, \mathbf{H}^k)$, and $\overline{\mathbf{H}} := \mathbf{H}^k - \frac{1}{d_k} \nabla_{\mathbf{H}} F(\mathbf{W}^k, \mathbf{H}^k)$.

According to Proposition 2 and Proposition 3 in references [30], we can know the closed solution of Eq. (16) and (17) can be obtained as follows:

$$P_f(\overline{\mathbf{W}}) := RS_k(P_+(\overline{\mathbf{W}})), \quad (18)$$

$$P_g(\overline{\mathbf{H}}) := P_+(\overline{\mathbf{H}}). \quad (19)$$

Then we can give the algorithm 3 for solving Eq. (9):

Algorithm 3 accPALM algorithm for solving Eq. (9)

Require: $\mathbf{X} \in \mathbb{R}^{p \times n}$.

Ensure: $\mathbf{W} \in \mathbb{R}^{p \times r}$ and $\mathbf{H} \in \mathbb{R}^{r \times n}$.

- 1: Initialization: $(\mathbf{W}^{-1}, \mathbf{H}^{-1}) = (\mathbf{W}^0, \mathbf{H}^0), \beta_0 \in [0, \beta_{\max}], \beta_{\max} < 1, k = 0$.
 - 2: **repeat**
 - 3: $\widetilde{\mathbf{W}}^k = \mathbf{W}^k + \beta_k(\mathbf{W}^k - \mathbf{W}^{k-1})$
 - 4: $c_k = \|\mathbf{H} \mathbf{H}^T\|_2$
 - 5: $\mathbf{W}^{k+1} = RS_k \left(P_+ \left(\widetilde{\mathbf{W}}^k - \frac{1}{c_k} \nabla_{\mathbf{W}} F(\widetilde{\mathbf{W}}^k, \mathbf{H}^k) \right) \right)$
 - 6: $\widetilde{\mathbf{H}}^k = \mathbf{H}^k + \beta_k(\mathbf{H}^k - \mathbf{H}^{k-1})$
 - 7: $d_k = \|\mathbf{W}^T \mathbf{W}^T\|_2 + \|2\lambda \mathbf{L}^T\|_2$
 - 8: $\mathbf{H}^{k+1} = P_+ \left(\widetilde{\mathbf{H}}^k - \frac{1}{d_k} \nabla_{\mathbf{H}} F(\mathbf{W}^{k+1}, \widetilde{\mathbf{H}}^k) \right)$
 - 9: **if** $F(\mathbf{W}^{k+1}, \mathbf{H}^{k+1}) \leq F(\mathbf{W}^k, \mathbf{H}^k) - \rho_0 \|(\mathbf{W}^{k+1} - \widetilde{\mathbf{W}}^k, \mathbf{H}^{k+1} - \widetilde{\mathbf{H}}^k)\|^2$ **then**
 - 10: Compute β_{k+1}
 - 11: **else**
 - 12: $\widetilde{\mathbf{H}}^k = \mathbf{H}^k, \widetilde{\mathbf{W}}^k = \mathbf{W}^k$
 - 13: repeat 5 and 8, compute β_{k+1}
 - 14: **end if**
 - 15: Set $k = k + 1$
 - 16: **until** $\frac{\|(\mathbf{W}^k, \mathbf{H}^k) - (\mathbf{W}^{k-1}, \mathbf{H}^{k-1})\|}{\|(\mathbf{W}^{k-1}, \mathbf{H}^{k-1})\|} < \epsilon$.
 - 17: **return** $\mathbf{W} := \mathbf{W}^k$ and $\mathbf{H} := \mathbf{H}^k$
-

In steps 10 and 13 of Algorithm 3, the update method for the extrapolation parameter β is not explicitly provided. We can choose to fix β , or dynamically adapt the parameters during the iteration process, similar to Algorithm 2. Through experiments detailed in the subsequent sections, we observe that adaptively updating the parameter β yields improved results. Unless otherwise specified, we will employ the dynamic update scheme for β in the following sections.

3.3 Convergence analysis

The convergence proof for the PALM algorithm has been presented in [24]. Our GNMF- ℓ_{20} framework adheres to the basic assumptions of PALM, ensuring that the convergence properties remain consistent with those established in [24]. Furthermore, we provide a convergence proof for the accPALM Algorithm (3), the main ideas of the proof are similar to [32]. Before proceeding with the formal proof of Algorithm 3, we introduce several foundational assumptions [33].

Assumption 1. (i) $f : \mathbb{R}^{p \times r} \rightarrow (-\infty, +\infty]$ and $g : \mathbb{R}^{r \times n} \rightarrow (-\infty, +\infty]$ are proper and lower semicontinuous functions.
(ii) $\inf_{\mathbb{R}^{p \times r} \times \mathbb{R}^{r \times n}} J > -\infty$, $\inf_{\mathbb{R}^{p \times r}} f > -\infty$ and $\inf_{\mathbb{R}^{r \times n}} g > -\infty$.
(iii) $F : \mathbb{R}^{p \times r} \times \mathbb{R}^{r \times n} \rightarrow \mathbb{R}$ is a C^1 function. The partial gradient $\nabla_W F(W, H)$ is globally Lipschitz with moduli L_W , and for any $W_1, W_2 \in \mathbb{R}^{p \times r}$, we have

$$\|\nabla_W F(W_1, H) - \nabla_W F(W_2, H)\| \leq L_W \|W_1 - W_2\|. \quad (20)$$

Likewise, we have a similar conclusion for $\nabla_H F(W, H)$ and L_H .

Lemma 1. (Convergence properties) Suppose that Assumption 1 holds. Let $\{(W^k, H^k)\}$ be a sequence generated by Algorithm 3. The following assertions hold.

(i) The sequences $J(W^k, H^k)$ is monotonically nonincreasing and in particular

$$\begin{aligned} & J(W^{k+1}, H^{k+1}) \\ & \leq J(\widetilde{W}^k, \widetilde{H}^k) - \rho_0 \|(W^{k+1} - \widetilde{W}^k, H^{k+1} - \widetilde{H}^k)\|^2, \end{aligned} \quad (21)$$

where $\rho_0 = \min\{\frac{1}{2}(c_k - L_W), \frac{1}{2}(d_k - L_H)\}$.

(ii) We have

$$\lim_{k \rightarrow \infty} \|W^{k+1} - \widetilde{W}^k\| = 0, \quad \lim_{k \rightarrow \infty} \|H^{k+1} - \widetilde{H}^k\| = 0. \quad (22)$$

Proof. (i) According to Lemma 2 of reference [24] and the iterative format of W and H , we can draw the following conclusions:

$$\begin{aligned} & F(W^{k+1}, \widetilde{H}^k) + f(W^{k+1}) \\ & \leq F(\widetilde{W}^k, \widetilde{H}^k) + f(\widetilde{W}^k) - \frac{1}{2}(c_k - L_W)\|W^{k+1} - \widetilde{W}^k\|^2, \end{aligned} \quad (23)$$

$$\begin{aligned} & F(W^{k+1}, H^{k+1}) + g(H^{k+1}) \\ & \leq F(W^{k+1}, \widetilde{H}^k) + g(\widetilde{H}^k) - \frac{1}{2}(d_k - L_H)\|H^{k+1} - \widetilde{H}^k\|^2. \end{aligned} \quad (24)$$

Adding the above two inequalities, we get

$$\begin{aligned} & J(W^{k+1}, H^{k+1}) \\ & \leq J(\widetilde{W}^k, \widetilde{H}^k) - \rho_0 \|(W^{k+1} - \widetilde{W}^k, H^{k+1} - \widetilde{H}^k)\|^2. \end{aligned} \quad (25)$$

From Algorithm 3, we can observe that the updates of W^{k+1} and H^{k+1} are derived from either steps 5 and 8 or step 13 in Algorithm 3. Let us consider two cases. If the updates of W^{k+1} and H^{k+1} are obtained from steps 5 and 8, the conditional statement (step 9) implies that the objective function decreases in this iteration. If the updates of W^{k+1} and H^{k+1} are obtained from step 13, then Eq. (25) will degenerate into

$$\begin{aligned} & J(W^{k+1}, H^{k+1}) \\ & \leq J(W^k, H^k) - \rho_0 \|(W^{k+1} - \widetilde{W}^k, H^{k+1} - \widetilde{H}^k)\|^2. \end{aligned} \quad (26)$$

It is evident that the objective function also remains non-increasing in this iteration. Thus, we can conclude that the objective function value is non-increasing as the iterations progress. And because the objective function is lower bounded (see Assumption 1), the sequence $J(W^k, H^k)$ is convergent.

(ii) According to the conclusion of Lemma 1(i) and the conditional statement (step 9), we know that no matter which step W^{k+1} and H^{k+1} are obtained from, Eq. (26) holds, that is

$$\begin{aligned} & \rho_0 \|(W^{k+1} - \widetilde{W}^k, H^{k+1} - \widetilde{H}^k)\|^2 \\ & \leq J(W^k, H^k) - J(W^{k+1}, H^{k+1}). \end{aligned} \quad (27)$$

The above Eq. (27) can be accumulated from $k = 0$ to K ,

$$\begin{aligned} & \sum_{k=0}^K \rho_0 \|(W^{k+1} - \widetilde{W}^k, H^{k+1} - \widetilde{H}^k)\|^2 \\ & \leq J(W^0, H^0) - J(W^{K+1}, H^{K+1}) \\ & \leq J(W^0, H^0) - J^* < \infty. \end{aligned}$$

Let $K \rightarrow \infty$, we know

$$\lim_{k \rightarrow \infty} \rho_0 \|(W^{k+1} - \widetilde{W}^k, H^{k+1} - \widetilde{H}^k)\|^2 = 0,$$

hence

$$\lim_{k \rightarrow \infty} \|W^{k+1} - \widetilde{W}^k\| = 0, \quad \lim_{k \rightarrow \infty} \|H^{k+1} - \widetilde{H}^k\| = 0. \quad (28)$$

This means the Lemma 1 is true. \square

Lemma 2. (A subgradient lower bound for the iterates gap) Suppose that Assumption 1 hold. Let $\{(W^k, H^k)\}$, $\{(\widetilde{W}^k, \widetilde{H}^k)\}$ be the sequences generated by Algorithm 2. For each integer $k \geq 1$, define

$$\begin{aligned} p_W^{k+1} &= \nabla_W F(W^{k+1}, H^{k+1}) - \nabla_W F(\widetilde{W}^k, \widetilde{H}^k) \\ & \quad + c_k(\widetilde{W}^k - W^{k+1}), \end{aligned} \quad (29)$$

$$\begin{aligned} p_H^{k+1} &= \nabla_H F(W^{k+1}, H^{k+1}) - \nabla_H F(W^{k+1}, \widetilde{H}^k) \\ & \quad + d_k(\widetilde{H}^k - H^{k+1}), \end{aligned} \quad (30)$$

then $q_W^{k+1} \in \partial_W J(W^{k+1}, H^{k+1})$, $p_H^{k+1} \in \partial_H J(W^{k+1}, H^{k+1})$ and there exists $\rho > 0$ such that

$$\|(p_W^{k+1}, p_H^{k+1})\| \leq \rho \|(W^{k+1} - \widetilde{W}^k, H^{k+1} - \widetilde{H}^k)\|. \quad (31)$$

Proof. From the iterative scheme of W , we can get

$$\begin{aligned} W^{k+1} &\in \arg \min_{W \in \mathbb{R}^{p \times r}} \{ \langle W - \widetilde{W}^k, \nabla_W F(\widetilde{W}^k, \widetilde{H}^k) \rangle \\ & \quad + \frac{c_k}{2} \|W - \widetilde{W}^k\| + f(W) \}, \end{aligned} \quad (32)$$

By optimality condition yields, we have

$$\nabla_W F(\widetilde{W}^k, \widetilde{H}^k) + c_k(W^{k+1} - \widetilde{W}^k) + u^{k+1} = 0, \quad (33)$$

where $u^{k+1} \in \partial f(W^{k+1})$. It follows that

$$\begin{aligned} p_W^{k+1} &= \nabla_W F(W^{k+1}, H^{k+1}) - \nabla_W F(\widetilde{W}^k, \widetilde{H}^k) \\ & \quad + c_k(\widetilde{W}^k - W^{k+1}) \\ & = \nabla_W F(W^{k+1}, H^{k+1}) + u^{k+1} \in \partial_W J(W^{k+1}, H^{k+1}). \end{aligned} \quad (34)$$

In a similar way, we know

$$\begin{aligned} p_H^{k+1} &= \nabla_H F(W^{k+1}, H^{k+1}) - \nabla_H F(W^{k+1}, \widetilde{H}^k) \\ & \quad + d_k(\widetilde{H}^k - H^{k+1}) \\ & = \nabla_H F(W^{k+1}, H^{k+1}) + v^{k+1} \in \partial_H J(W^{k+1}, H^{k+1}), \end{aligned} \quad (35)$$

where $v^{k+1} \in \partial g(H^{k+1})$. There exists $M > 0$ such that

$$\begin{aligned} \|p_W^{k+1}\| &\leq c_k \|\widetilde{W}^k - W^{k+1}\| + \|\nabla_W F(W^{k+1}, H^{k+1}) \\ & \quad - \nabla_W F(\widetilde{W}^k, \widetilde{H}^k)\| \\ &\leq c_k \|\widetilde{W}^k - W^{k+1}\| + M(\|W^{k+1} - \widetilde{W}^k\| \\ & \quad + \|H^{k+1} - \widetilde{H}^k\|) \\ & = (M + c_k) \|\widetilde{W}^k - W^{k+1}\| + M \|H^{k+1} - \widetilde{H}^k\| \\ &\leq (2M + c_k) \|(W^{k+1} - \widetilde{W}^k, H^{k+1} - \widetilde{H}^k)\|. \end{aligned}$$

By the same way, because $\nabla_H F$ is Lipschitz continuous, we have

$$\begin{aligned} \|p_H^{k+1}\| &\leq d_k \|\tilde{H}^k - H^{k+1}\| + \|\nabla_H F(W^{k+1}, H^{k+1}) \\ &\quad - \nabla_H F(W^{k+1}, \tilde{H}^k)\| \\ &\leq d_k \|\tilde{H}^k - H^{k+1}\| + d_k \|H^{k+1} - \tilde{H}^k\| \\ &= 2d_k \|H^{k+1} - \tilde{H}^k\|, \end{aligned}$$

hence

$$\begin{aligned} \|(p_W^{k+1}, p_H^{k+1})\| &\leq \|p_W^{k+1}\| + \|p_H^{k+1}\| \\ &\leq \rho \| (W^{k+1} - \tilde{W}^k, H^{k+1} - \tilde{H}^k) \|. \end{aligned} \quad (36)$$

This means the Lemma 2 is true. \square

In the following outcomes, we summarize several properties of the set of limit points. For convenience, we often use the notation $z^k := (W^k, H^k)$, $\forall k \geq 0$ in the following text. We first give the definition of the limit points set, let $\{z^k\}$, where $k \in \mathbb{N}$, be the sequence generated by Algorithm 3 from the initial point z^0 . The collection of all limit points is denoted by $\omega(z^0)$, which is defined as follows:

$$\begin{aligned} \omega(z^0) &= \{\bar{z} = (\bar{W}, \bar{H}) \in \mathbb{R}^{p \times r} \times \mathbb{R}^{r \times n} : \\ &\exists \text{ a sequence of integers } \{k_j\}_{j \in \mathbb{N}} \text{ such that } z^{k_j} \rightarrow \bar{z}, j \rightarrow \infty\}. \end{aligned} \quad (37)$$

Lemma 3. (Subsequence convergence) *Let Assumption 1 holds, $\{z_k\}$ is the sequence generated by Algorithm 3, the following assertion hold.*

- (i) $\emptyset \neq \omega(z^0) \subset \text{crit}J$.
- (ii) $\omega(z^0)$ is a nonempty and compact set, and the objective function J is finite and constant on $\omega(z^0)$.
- (iii) We have

$$\lim_{k \rightarrow \infty} \text{dist}(z^k, \omega(z^0)) = 0.$$

Proof. (i) From Lemma 1, we know

$$\lim_{j \rightarrow \infty} \|W^{k_j} - \tilde{W}^{k_j-1}\| = 0, \lim_{j \rightarrow \infty} \|H^{k_j} - \tilde{H}^{k_j-1}\| = 0, \quad (38)$$

hence

$$\begin{aligned} \lim_{j \rightarrow \infty} W^{k_j} &= \lim_{j \rightarrow \infty} \tilde{W}^{k_j-1} = \bar{W}, \\ \lim_{j \rightarrow \infty} H^{k_j} &= \lim_{j \rightarrow \infty} \tilde{H}^{k_j-1} = \bar{H}. \end{aligned} \quad (39)$$

From Lemma 2, we have

$$\|(p_W^{k_j}, p_H^{k_j})\| \leq \rho \| (W^{k_j} - \tilde{W}^{k_j-1}, H^{k_j} - \tilde{H}^{k_j-1}) \|, \quad (40)$$

further we can conclude

$$(p_W^{k_j}, p_H^{k_j}) \rightarrow (0, 0) \text{ as } j \rightarrow \infty. \quad (41)$$

According to $\lim_{j \rightarrow \infty} j(W^{k_j}, H^{k_j}) = j(\bar{W}, \bar{H})$, $(q_W^{k_j}, p_H^{k_j}) \in \partial J(W^{k_j}, H^{k_j})$ and ∂J closed, we get $(0, 0) \in \partial J(\bar{W}, \bar{H})$, this proves that the $\bar{z} = (\bar{W}, \bar{H})$ is a critical point of J , that is to say $\omega(z^0) \subset \text{crit}J$.

(ii) The boundedness of the sequence $\{z^k\}$ implies that the set $\omega(z^0)$ is not empty. Furthermore, the expression for $\omega(z^0)$ can be redefined as the intersection of compact sets

$$\omega(z^0) = \bigcap_{s \in \mathbb{N}} \overline{\bigcup_{k \geq s} \{z^k\}}, \quad (42)$$

demonstrating that $\omega(z^0)$ forms a compact set and for any $\bar{z} = (\bar{W}, \bar{H}) \in \omega(z^0)$, there exist a subsequence $\{z^{k_j}\}$ such that

$$\lim_{j \rightarrow \infty} z^{k_j} = \bar{z}. \quad (43)$$

Since f and g are lower semicontinuous, we obtain that

$$\liminf_{j \rightarrow \infty} f(W^{k_j}) \geq f(\bar{W}), \liminf_{j \rightarrow \infty} g(H^{k_j}) \geq g(\bar{H}). \quad (44)$$

From the iterative step in Algorithm 3, we know that for all integer k

$$\begin{aligned} W^{k+1} &\in \text{argmin}_W \{ \langle W - \tilde{W}^k, \nabla_W F(\tilde{W}^k, H^k) \rangle + \\ &\quad \frac{c_k}{2} \|W - \tilde{W}^k\|^2 + f(W) \}, \end{aligned} \quad (45)$$

letting $W = \bar{W}$, we can get

$$\begin{aligned} \langle W^{k+1} - \tilde{W}^k, \nabla_W F(\tilde{W}^k, H^k) \rangle + \frac{c_k}{2} \|W^{k+1} - \tilde{W}^k\|^2 + \\ f(W^{k+1}) \leq \langle \bar{W} - \tilde{W}^k, \nabla_W F(\tilde{W}^k, H^k) \rangle + \\ \frac{c_k}{2} \|\bar{W} - \tilde{W}^k\|^2 + f(\bar{W}). \end{aligned} \quad (46)$$

Then letting $k = k_j - 1$,

$$\begin{aligned} \limsup_{j \rightarrow \infty} f(W^{k_j}) \\ \leq \limsup_{j \rightarrow \infty} (\langle \bar{W} - \tilde{W}^{k_j-1}, \nabla_W F(\tilde{W}^{k_j-1}, H^{k_j-1}) \rangle \\ + \frac{c_k}{2} \|\bar{W} - \tilde{W}^{k_j-1}\|^2) + f(\bar{W}), \end{aligned} \quad (47)$$

since $\tilde{W}^{k_j-1} \rightarrow \bar{W}$ as $j \rightarrow \infty$, Eq.(47) reduces to

$$\limsup_{j \rightarrow \infty} f(W^{k_j}) \leq f(\bar{W}), \quad (48)$$

thus, by combining Eq.(44), we obtain

$$\lim_{j \rightarrow \infty} f(W^{k_j}) = f(\bar{W}). \quad (49)$$

Applying a similar argument to g and H^k , we get

$$\lim_{j \rightarrow \infty} g(H^{k_j}) = g(\bar{H}). \quad (50)$$

Considering the continuity of F (see Assumption 1), we can finally obtain

$$\lim_{j \rightarrow \infty} J(z^{k_j}) = J(\bar{z}), \quad (51)$$

which means that J is constant on $\omega(z^0)$.

(iii) This term is a basic result of the limit point definition, or we can use the strategy of disproving. Suppose $\lim_{k \rightarrow \infty} \text{dist}(z^k, \omega(z^0)) \neq 0$, then there is a subsequence $\{z^{k_m}\}$ and a constant M greater than zero, so that

$$\|z^{k_m} - \bar{z}\| \geq \text{dist}(z^{k_m}, \omega(z^0)) > M, \forall \bar{z} \in \omega(z^0). \quad (52)$$

On the other hand, $\{z^{k_m}\}$ is bounded and has a subsequence $\{z^{k_{m_j}}\}$ converges to a point in $\omega(z^0)$, so

$$\lim_{k \rightarrow \infty} \text{dist}(z^k, \omega(z^0)) = 0. \quad (53)$$

This means the Lemma 3 is true. \square

Theorem 1. (Global convergence) *Assuming that J is a KL function and $\{z^k\}$ is a sequence generated by algorithm 3 with initial point z^0 . Suppose Assumptions 1 holds then it has the following properties:*

- (i) $\sum_{k=0}^{\infty} \|z^{k+1} - z^k\| < \infty$.
- (ii) The sequence $\{z^k\}$ converges to the critical point of J .

Proof. (i) Since $\{J(z^k)\}$ is a non-increasing sequence, and from Lemma 3 we know that $\lim_{k \rightarrow \infty} J(z^k) = J(\bar{z})$, it is clear that

$J(\bar{z}) < J(z^k)$ for all $k > 0$ and for any $\eta > 0$, there exists a positive integer k_0 such that $J(z^{k_0}) < J(\bar{z}) + \eta$, hence for all $k > k_0$ we have

$$z^k \in \left[J(\bar{z}) < J(z^k) < J(\bar{z}) + \eta \right]. \quad (54)$$

From Lemma 3 (iv) we know that $\lim_{k \rightarrow \infty} \text{dist}(z^k, \omega(z^0)) = 0$, thus for any $\epsilon > 0$ there exists a positive integer k_1 such that

$$\text{dist}(z^k, \omega(z^0)) < \epsilon, \forall k > k_1. \quad (55)$$

Based on Eq. (54) and (55), it is observed that by letting $l = \max\{k_0, k_1\}$, for any $k > l$, we have

$$z^k \in \{z \mid \text{dist}(z^k, \omega(z^0)) < \epsilon\} \cap \left[J(\bar{z}) < J(z^{k_0}) < J(\bar{z}) + \eta \right]. \quad (56)$$

Since J is finite and constant on the nonempty and compact set $\omega(z^0)$ (see Lemma 3), according to Lemma 6 in [24], there exists a concave function φ , for any $k > l$ we get that

$$\varphi' \left(J(z^k) - J(\bar{z}) \right) \text{dist}(0, \partial J(z^k)) \geq 1. \quad (57)$$

From Lemma 2, we have

$$\begin{aligned} \text{dist}(0, \partial J(z^k)) &\leq \rho \left\| (W^k - \widetilde{W}^{k-1}, H^k - \widetilde{H}^{k-1}) \right\| \\ &= \rho \left\| z^k - \omega^{k-1} \right\|, \end{aligned} \quad (58)$$

where $\omega^{k-1} := (\widetilde{W}^{k-1}, \widetilde{H}^{k-1})$, combine Eq. (57) and (58), we get that

$$\varphi' \left(J(z^k) - J(\bar{z}) \right) \geq \frac{1}{\rho \left\| z^k - \omega^{k-1} \right\|}. \quad (59)$$

From the convexity of φ we get

$$\begin{aligned} \varphi \left(J(z^{k+1}) - J(\bar{z}) \right) - \varphi \left(J(z^k) - J(\bar{z}) \right) \\ \leq \varphi' \left(J(z^k) - J(\bar{z}) \right) \left(J(z^{k+1}) - J(z^k) \right), \end{aligned} \quad (60)$$

and from Lemma 1 and Eq. (59) we have

$$\begin{aligned} \varphi \left(J(z^k) - J(\bar{z}) \right) - \varphi \left(J(z^{k+1}) - J(\bar{z}) \right) \\ \geq \varphi' \left(J(z^k) - J(\bar{z}) \right) \left(J(z^k) - J(z^{k+1}) \right) \\ \geq \frac{\rho_0 \left\| z^{k+1} - \omega^k \right\|^2}{\rho \left\| z^k - \omega^{k-1} \right\|}. \end{aligned} \quad (61)$$

For convenience, we define $\Delta_k = \varphi \left(J(z^k) - J(\bar{z}) \right)$, let $C = \frac{\rho}{\rho_0}$, then Eq. (61) can be simplified as

$$\Delta_k - \Delta_{k+1} \geq \frac{\left\| z^{k+1} - \omega^k \right\|^2}{C \left\| z^k - \omega^{k-1} \right\|}. \quad (62)$$

It follows that

$$\left\| z^{k+1} - \omega^k \right\|^2 \leq C(\Delta_k - \Delta_{k+1}) \left\| z^k - \omega^{k-1} \right\|, \quad (63)$$

$$2 \left\| z^{k+1} - \omega^k \right\| \leq C(\Delta_k - \Delta_{k+1}) + \left\| z^k - \omega^{k-1} \right\|. \quad (64)$$

Summing up Eq. (64) for $k = l + 1, \dots, K$ yields

$$\begin{aligned} 2 \sum_{k=l+1}^K \left\| z^{k+1} - \omega^k \right\| \\ \leq \sum_{k=l+1}^K \left\| z^k - \omega^{k-1} \right\| + C(\Delta_{l+1} - \Delta_{K+1}) \\ \leq \left\| z^{l+1} - \omega^l \right\| + \sum_{k=l+1}^K \left\| z^{k+1} - \omega^k \right\| + C(\Delta_{l+1} - \Delta_{K+1}), \end{aligned} \quad (65)$$

and hence, let $K \rightarrow \infty$, we get

$$\sum_{k=l+1}^{\infty} \left\| z^{k+1} - \omega^k \right\| \leq \left\| z^{l+1} - \omega^l \right\| + C\Delta_{l+1} < \infty. \quad (66)$$

This shows that the sequence $\{z^k\}$ is finite, and

$$\sum_{k=0}^{\infty} \left\| z^{k+1} - \omega^k \right\| < \infty. \quad (67)$$

Study the iteration point $\omega^k = (\widetilde{W}^k, \widetilde{H}^k)$ in Algorithm 3. We note that if $(\widetilde{W}^k, \widetilde{H}^k)$ is generated by (5)(8), then

$$\begin{aligned} (W^{k+1} - \widetilde{W}^k, H^{k+1} - \widetilde{H}^k) \\ = (W^{k+1} - W^k - \beta_k(W^k - W^{k-1}), \\ , H^{k+1} - H^k - \beta_k(H^k - H^{k-1})) \\ = z^{k+1} - z^k - \beta_k(z^k - z^{k-1}). \end{aligned} \quad (68)$$

If $(\widetilde{W}^k, \widetilde{H}^k)$ is generated by (13), then

$$\begin{aligned} (W^{k+1} - \widetilde{W}^k, H^{k+1} - \widetilde{H}^k) &= (W^{k+1} - W^k, H^{k+1} - H^k) \\ &= z^{k+1} - z^k. \end{aligned} \quad (69)$$

Combining Eq. (68) and (69) we can get

$$\left\| z^{k+1} - \omega^k \right\| \geq \left\| z^{k+1} - z^k \right\| - \beta_k \left\| z^k - z^{k-1} \right\|, \quad (70)$$

and summing up Eq. (70) for $k = l + 1, \dots, K$ yields

$$\begin{aligned} \sum_{k=l+1}^K \left\| z^{k+1} - z^k \right\| - \sum_{k=l+1}^K \beta_k \left\| z^k - z^{k-1} \right\| \\ \leq \sum_{k=l+1}^K \left\| z^{k+1} - \omega^k \right\| < \infty, \end{aligned} \quad (71)$$

and hence

$$\begin{aligned} \sum_{k=l+1}^K \left\| z^{k+1} - z^k \right\| - \sum_{k=l+1}^K \beta_k \left\| z^k - z^{k-1} \right\| \\ \geq \sum_{k=l+1}^K \left\| z^{k+1} - z^k \right\| - \beta_{\max} \sum_{k=l+1}^K \left\| z^{k+1} - z^k \right\| - \beta_k \left\| z^{l+1} - z^l \right\| \\ = (1 - \beta_{\max}) \sum_{k=l+1}^K \left\| z^{k+1} - z^k \right\| - \beta_k \left\| z^{l+1} - z^l \right\|. \end{aligned} \quad (72)$$

Combining Eq. (71) and (72) we have

$$(1 - \beta_{\max}) \sum_{k=l+1}^K \left\| z^{k+1} - z^k \right\| < \infty.$$

Let $K \rightarrow \infty$, from $0 \leq \beta_{max} < 1$ we can get

$$\sum_{k=l+1}^{\infty} \|z^{k+1} - z^k\| < \infty, \quad (73)$$

which means

$$\sum_{k=0}^{\infty} \|z^{k+1} - z^k\| < \infty. \quad (74)$$

(ii) Eq. (74) shows that with $m > n \geq l$, we have

$$\begin{aligned} \|z^m - z^n\| &= \left\| \sum_{k=n}^{m-1} (z^{k+1} - z^k) \right\| \leq \sum_{k=n}^{m-1} \|z^{k+1} - z^k\| \\ &< \sum_{k=n}^{\infty} \|z^{k+1} - z^k\|. \end{aligned} \quad (75)$$

From Eq. (75), we get $\|z^m - z^n\|$ converges to zero as $n \rightarrow \infty$, it follows that $\{z^k\}$ is a Cauchy sequence and thus a convergent sequence. From Lemma 3 (iii), it can be concluded that $\{z^k\}$ converges to a critical point of J . \square

Theorem 2. (Convergence rate) *Let Assumption 1 hold and the desingularizing function has the form of $\varphi(t) = \frac{c}{\theta} t^\theta$ with $\theta \in (0, 1]$, $c > 0$. Let $J(z) = J^*$ for all $z \in \omega(z^0)$, and denote $r_k := J(z^k) - J^*$. Then the sequence $\{r_k\}$ satisfies for k_2 large enough:*

- 1) If $\theta = 1$, then r_k reduces to zero in finite steps;
- 2) If $\theta \in [\frac{1}{2}, 1)$, then there exist a constant $P \in [0, 1)$ such that $r_k \leq r_{k_2} P^{k-k_2}$;
- 3) If $\theta \in (0, \frac{1}{2})$, then there exist a constant $Q > 0$ such that $r_k \leq \left(\frac{Q}{(k-k_2)(1-2\theta)} \right)^{\frac{1}{1-2\theta}}$.

Proof. Checking the assumptions of Theorem 3 in reference [34], we observe that all assumptions required in Algorithm 3 are clearly satisfied, so Theorem 2 holds. \square

4 EXPERIMENTS

We evaluate the effectiveness of the proposed $\text{GNMF}_{\ell_{20}}$ method for the clustering task and compare it with state-of-the-art matrix factorization methods, as well as the k-means and sparse k-means methods. The competing methods considered in the evaluation are as follows:

- NMF: Non-negative Matrix Factorization.
- NMF_{ℓ_0} : NMF with ℓ_0 sparsity constraint.
- $\text{SNMF}_{\ell_{20}}$: Sparse NMF with ℓ_{20} sparsity constraint [30].
- $\text{SNMF}_{\ell_{c0}}$: Sparse NMF with ℓ_{c0} sparsity constraint [30].
- GNMF: Graph NMF.
- GNMF_{ℓ_0} : Graph NMF with ℓ_0 sparsity constraint.
- Kmeans: K-means clustering algorithm.
- Kmeans_{ℓ_0} : K-means clustering with ℓ_0 sparsity constraint [35].

4.1 Evaluation metrics

In the experiment, we use Normalized Mutual Information (NMI) and Accuracy (ACC) as key metrics to evaluate clustering quality and accuracy.

Normalized Mutual Information (NMI) [36]: NMI is a metric used to measure the similarity between the clustering results and the ground truth labels. NMI ranges from 0 to 1, where a value

closer to 1 indicates a higher consistency between the clustering results and the ground truth labels.

The formula to calculate NMI is as follows:

$$\text{NMI} = \frac{2 \times I(C, T)}{H(C) + H(T)}, \quad (76)$$

where C represents the clustering results, T represents the ground truth labels, $I(C, T)$ denotes the mutual information between C and T , and $H(C)$ and $H(T)$ represent the entropy of C and T , respectively.

Accuracy is a metric used to measure the correctness of the clustering results. It represents the ratio of correctly classified samples to the total number of samples. Accuracy ranges from 0 to 1, where a value closer to 1 indicates a higher accuracy of the clustering results. The formula to calculate accuracy is as follows:

$$\text{Accuracy} = \frac{\sum_{i=1}^n h(y_i, \hat{y}_i)}{n}, \quad (77)$$

where n represents the total number of samples, y_i represents the true labels of the i -th sample, \hat{y}_i represents the clustering result of the i -th sample, and $h(y_i, \hat{y}_i)$ represents an indicator function that is 1 when y_i and \hat{y}_i are equal and 0 otherwise.

4.2 Application to synthetic data

We construct a synthetic dataset with three Gaussian clusters. Each cluster is generated by sampling from a multivariate Gaussian distribution with a specified mean and covariance matrix. The means of the three clusters are set as -2, 0, and 2, respectively, with a covariance matrix of identity. To introduce variability and noise into the dataset, we add random noise by generating samples from a normal distribution and appending them to the original data. The noise is added only to the last three rows of the dataset, while the rest of the data remains unchanged. For consistency and comparability across the dataset, a linear normalization is performed. This involves subtracting the minimum value from each data point and dividing the result by the range of values, transforming the data to a new scale from 0 to 1. Finally, we perturb the order of the last three rows by shuffling their columns randomly. And the synthetic data set we constructed is shown in Figure 2A.

In order to conduct experiments on the $\text{GNMF}_{\ell_{20}}$ method and achieve better results, we manually constructed the adjacency matrix for graph regularization. By customizing the adjacency matrix, we can incorporate prior knowledge or desired characteristics into the graph regularization process, thereby guiding the clustering algorithm to capture relevant information and improve clustering performance. Then we introduce the construction method of adjacency matrix as follows.

Firstly, we initialized a square matrix with zeros, representing the absence of connections between data points. Then, we divided the matrix into blocks corresponding to different clusters or groups in the dataset. Within each block, we randomly assigned non-zero values to represent the presence of connections between data points. The probabilities of assigning non-zero values were set according to a predefined distribution, reflecting the desired level of connectivity within each cluster. Finally, we ensured symmetry by setting the corresponding elements in the lower triangular part of the matrix equal to the corresponding elements in the upper triangular part.

We demonstrate the convergence performance of PALM and accPALM in solving the $\text{GNMF}_{\ell_{20}}$ problem on synthetic dataset

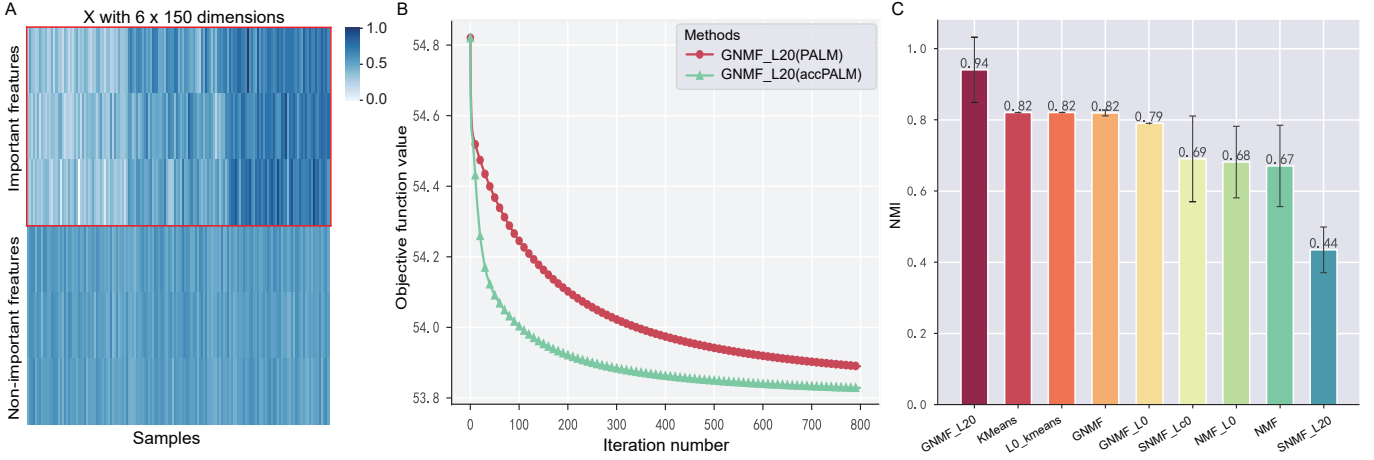


Figure 2. Results on the synthetic data. (A) Heatmap showing the synthetic data. (B) Convergence performance of PALM and accPALM for $\text{GNMf}_{\ell_{20}}$ and the initial value of the inertial parameter β of the acceleration method is 0.5. (C) Comparison of nine unsupervised clustering methods in terms of NMI on the synthetic data.

Table 1

Averaged performance of $\text{GNMf}_{\ell_{20}}$ with different algorithms in terms of $\text{Relative Error} = \frac{\|X - WH\|_F}{\|X\|_F}$ and running time (seconds) on the LIBRAS, UMIST and USPS datasets. The best results are highlighted in bold.

Data	LIBRAS data		UMIST data		JAFFE data	
	Relative Error	Time (seconds)	Relative Error	Time (seconds)	Relative Error	Time (seconds)
BPL	0.736	47.007	0.971	133.238	0.564	52.882
PALM	0.745	48.961	0.990	75.352	0.566	51.134
iPALM	0.746	47.758	0.991	78.736	0.604	60.445
accPALM	0.741	40.252	0.971	20.004	0.563	47.746

in Figure 2B. The results indicate that accPALM exhibits significantly faster convergence compared to the standalone PALM method. Subsequently, we compare the $\text{GNMf}_{\ell_{20}}$ method with other classical clustering algorithms, revealing that our approach outperforms the other classical methods on synthetic dataset (See Figure 2C). Our method excels in filtering out irrelevant features from the data matrix and the incorporation of graph structure further enhances its performance. Furthermore, we observed that the standard GNMf and SNMF $_{\ell_{20}}$ methods are less effective compared to $\text{GNMf}_{\ell_{20}}$. This underscores the performance improvement achieved through the combination of graph regularization and $\ell_{2,0}$ -norm constraints.

4.3 Application to real image datasets

This study evaluates the proposed method and competing methods on three real-world image datasets, as follows:

- **LIBRAS** dataset is a widely used dataset in sign language recognition research [37]. It consists of video sequences of Brazilian Sign Language (LIBRAS) gestures performed by different individuals. Each gesture is recorded from multiple viewpoints, capturing variations in hand shapes, movements, and orientations.
- **UMIST** dataset is a popular face recognition dataset. It contains grayscale images of faces from 20 different individuals, with varying poses, expressions, and lighting conditions.
- **JAFFE** dataset is a dataset for facial expression analysis. It consists of grayscale images of Japanese female faces

displaying seven different facial expressions: neutral, happiness, sadness, surprise, anger, disgust, and fear.

We demonstrate the convergence performance when solving the $\text{GNMf}_{\ell_{20}}$ model in Eq.(11) using PALM and accPALM on image data (Figure 3). When the extrapolation parameter β is 0, accPALM degenerates into the ordinary PALM algorithm. Across the three image datasets, various settings of extrapolation parameters exhibit similar impacts on convergence speed, and it is found that the convergence speed of our proposed accelerated method is significantly faster than that of the ordinary PALM method. And as the extrapolation parameter β of the acceleration method increases, the convergence speed of the objective function also becomes faster, and the convergence speed is fastest when the parameter β changes adaptively during the iteration process, so unless otherwise specified, the article The accPALM method adopts the strategy of β adaptive change.

We compare our proposed method with other commonly used optimization algorithms, including iPALM [26] and BPL [27], on three image datasets (Table 1). To ensure fairness, all these algorithms were initialized with the same random starting points. We conducted ten repetitions of each algorithm, with each repetition using a different randomly generated initial point. Additionally, we set the termination criterion for all algorithms as $\frac{\|(W^t, H^t) - (W^{t-1}, H^{t-1})\|}{\|(W^{t-1}, H^{t-1})\|} \leq 10^{-3}$. We compare the convergence speed and relative error of these methods, and the results demonstrated that accPALM exhibited the fastest convergence rate and excellent performance in terms of relative error. Specifically, in UMIST dataset, the accPALM algorithm demonstrates significantly reduced computation time compared to other algorithms,

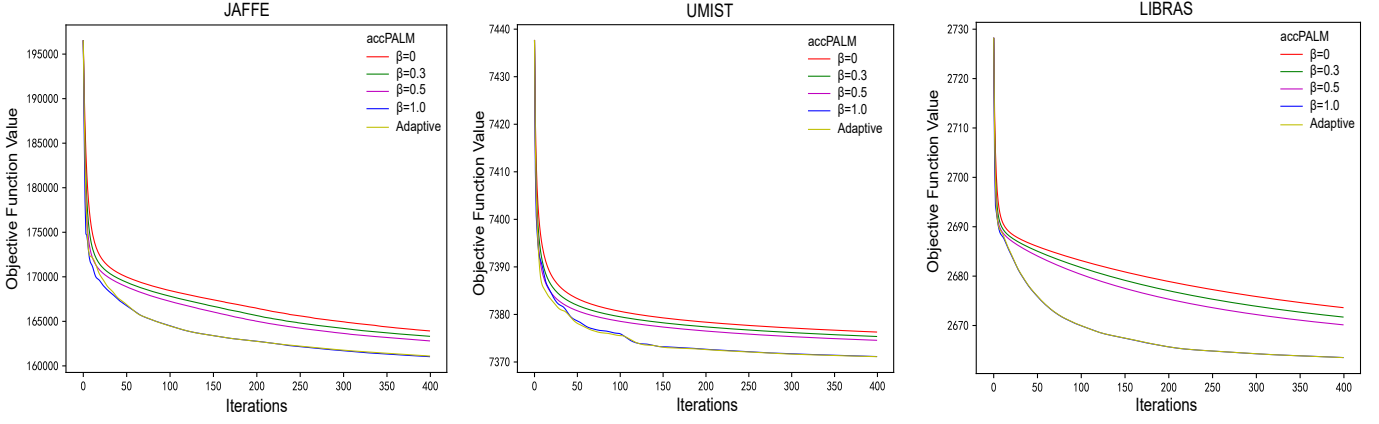


Figure 3. Convergence performance of accPALM with different parameters β for $\text{GNMF}_{\ell_{2,0}}$, where the first four lines represent the convergence performance when the extrapolation parameter β is fixed, and the last line represents the convergence performance when the extrapolation parameter β changes dynamically as the iteration proceeds.

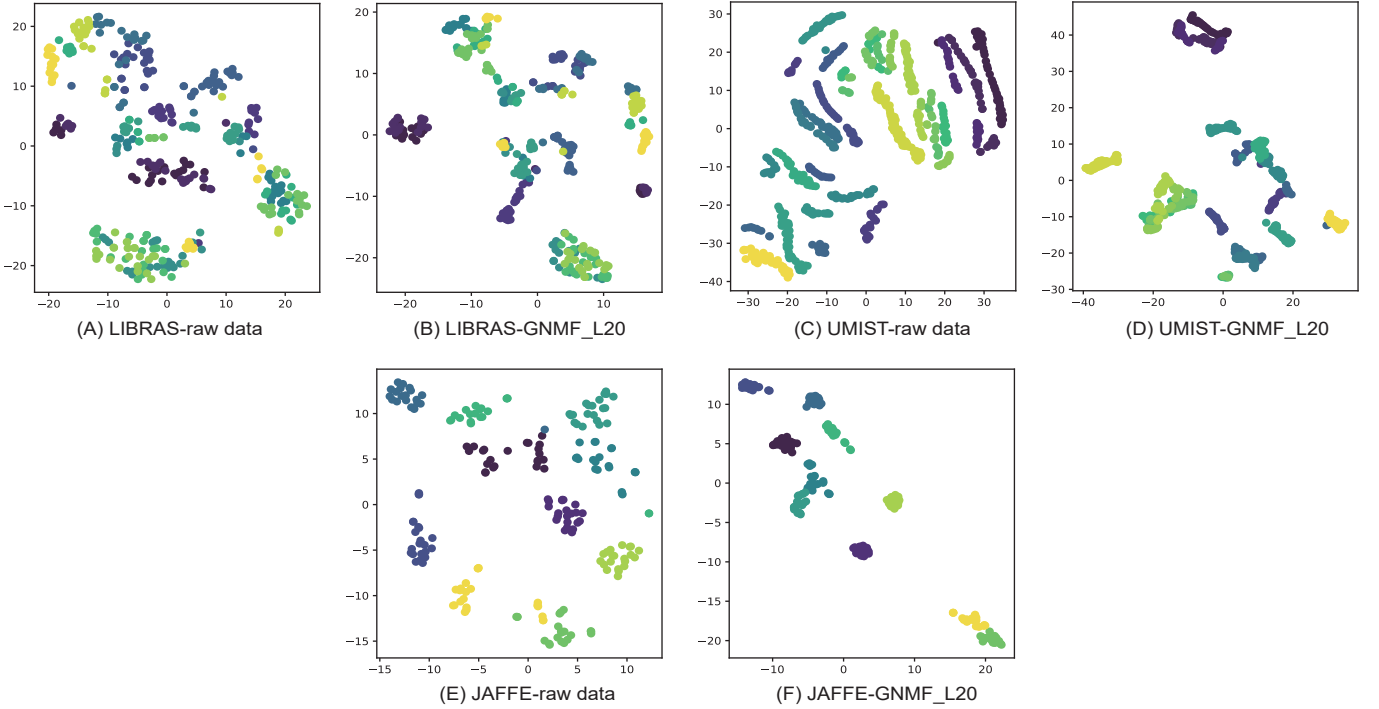


Figure 4. 2D visualization results via t-SNE. The comparison of the raw data and the clustering results of $\text{GNMF}_{\ell_{2,0}}$ on LIBRAS, UMIST and JAFFE datasets.

enhancing convergence speed while maintaining good relative error.

We evaluate the clustering performance of these methods from two aspects, NMI (Normalized Mutual Information) and ACC (Accuracy) (Table 2). We performed k-means clustering on the \mathbf{H} matrix resulting from matrix factorization to obtain the final clustering results. The clustering evaluations are presented in Table 2, where it is evident that our proposed $\text{GNMF}_{\ell_{2,0}}$ method outperforms the others. In detail, the incorporation of graph regularization has a positive impact on clustering. The clustering index of GNMf is approximately 5% to 15% higher compared to the conventional NMF method. However, we observed that the

enhancement of GNMf over NMF in the UMIST dataset is not pronounced. This could be attributed to the graph regularization module not effectively capturing the internal structure information of the data. The incorporation of $\ell_{2,0}$ -norm constraint, however, may capture crucial features, thus improving the clustering performance.

We also investigate the impact of the number of features on the algorithms' performance (Table 3). By selecting various numbers of features and observing the clustering evaluations in our experiments, we found that $\text{GNMF}_{\ell_{2,0}}$ consistently outperformed other methods across different feature counts. In the LIBRAS data set, we found that the clustering performance of $\text{GNMF}_{\ell_{2,0}}$

Table 2

Comparison in terms of (NMI % \pm std) and (ACC % \pm std) on the LIBRAS, UMIST and JAFFE datasets.

LIBRAS data	#Features	NMI \pm sd	ACC \pm sd
GNMF_ ℓ_{20}	40	65.66 \pm 1.45	50.42 \pm 2.59
NMF	all	59.45 \pm 1.61	48.03 \pm 2.20
NMF_ ℓ_0	/	59.07 \pm 0.92	48.36 \pm 1.39
NMF_ ℓ_{20}	40	58.08 \pm 1.92	45.61 \pm 1.96
NMF_ ℓ_{c0}	/	59.42 \pm 1.26	47.69 \pm 1.87
GNMF	all	65.28 \pm 1.30	49.28 \pm 1.62
GNMF_ ℓ_0	/	58.95 \pm 1.62	49.00 \pm 1.62
Kmeans	all	59.43 \pm 0.71	44.42 \pm 1.62
Kmeans_ ℓ_0	40	40.73 \pm 0.46	29.50 \pm 0.73
UMIST data	#Features	NMI \pm sd	ACC \pm sd
GNMF_ ℓ_{20}	50	74.76 \pm 2.48	54.37 \pm 3.07
NMF	all	61.13 \pm 1.24	42.50 \pm 1.73
NMF_ ℓ_0	/	61.97 \pm 2.00	39.97 \pm 1.55
NMF_ ℓ_{20}	2200	59.48 \pm 2.49	42.10 \pm 1.85
NMF_ ℓ_{c0}	/	61.32 \pm 1.07	40.09 \pm 1.63
GNMF	all	64.56 \pm 2.07	43.10 \pm 3.08
GNMF_ ℓ_0	/	74.09 \pm 0.86	54.42 \pm 1.67
Kmeans	all	65.34 \pm 1.45	43.63 \pm 1.83
Kmeans_ ℓ_0	50	50.66 \pm 1.38	36.70 \pm 0.97
JAFFE data	#Features	NMI \pm sd	ACC \pm sd
GNMF_ ℓ_{20}	50000	94.24 \pm 2.73	94.98 \pm 3.06
NMF	all	87.87 \pm 4.05	86.29 \pm 6.40
NMF_ ℓ_0	/	88.11 \pm 3.03	83.80 \pm 4.79
NMF_ ℓ_{20}	50000	86.24 \pm 2.11	84.84 \pm 2.59
NMF_ ℓ_{c0}	/	87.48 \pm 3.22	83.38 \pm 4.61
GNMF	all	92.26 \pm 4.30	90.89 \pm 6.27
GNMF_ ℓ_0	/	14.31 \pm 0.39	22.82 \pm 0.23
Kmeans	all	90.25 \pm 3.48	85.68 \pm 4.84
Kmeans_ ℓ_0	50000	46.26 \pm 0.58	33.99 \pm 1.15

generally gets better as the number of selected features increases. The clustering effectiveness peaks when the number of features reaches 50, suggesting that our method has identified the 50 most important features in the data, successfully mitigating noise interference.

Table 3

Comparison of (NMI %) averages with different number of characteristic number (k) on the LIBRAS, UMIST and JAFFE datasets.

LIBRAS data (k)	5	10	30	50	70	90
GNMF_ ℓ_{20}	48.63	59.58	66.53	66.30	65.34	64.50
NMF_ ℓ_{20}	23.89	44.89	58.33	59.61	59.82	59.04
Kmeans_ ℓ_0	32.13	36.40	46.39	51.86	57.28	59.00
UMIST data (k)	200	500	1000	1500	2000	2500
GNMF_ ℓ_{20}	72.35	69.73	67.19	65.61	64.86	65.63
NMF_ ℓ_{20}	49.46	56.88	59.11	60.47	58.69	59.27
Kmeans_ ℓ_0	61.18	65.92	65.05	65.02	65.79	65.28
JAFFE data (k)	5000	10000	30000	50000	60000	65000
GNMF_ ℓ_{20}	93.19	93.40	92.82	94.18	92.58	90.83
NMF_ ℓ_{20}	74.87	83.85	88.11	91.77	86.70	87.03
Kmeans_ ℓ_0	60.85	66.93	79.16	86.40	90.29	88.43

We further use the t-SNE algorithm to visualize the clustering results of the three data sets in 2-dimensional space [38], as shown in Figure 4. From Figure 4, we can know that compared with the original data, the data points are driven into different groups after GNMF_ ℓ_{20} clustering, and points from the same cluster become more concentrated.

5 CONCLUSION

In this paper, we present a GNMF model with $\ell_{2,0}$ -norm constraint and integrated feature selection and graph regularization into the NMF framework. We have known that $\ell_{2,0}$ -norm satisfies the KŁ property, allowing us to utilize the PALM algorithm to solve the nonconvex and non-smooth optimization problems associated with $\ell_{2,0}$ -norm constraint. Specifically, we have introduced the GNMF_ ℓ_{20} model and developed an accelerated version of PALM (accPALM) to solve it efficiently. Through extensive experiments on synthetic and real image datasets, we compare our proposed GNMF_ ℓ_{20} methods with competing methods for the clustering task. The results demonstrate the superior performance of our methods in terms of clustering accuracy and feature selection. Overall, our work contributes to the advancement of SSNMF models and their applications in clustering and feature selection tasks. The proposed algorithms have been supported by convergence theory and have demonstrated state-of-the-art performance. However, further research is needed to explore automatic parameter selection and global optimization solutions. In conclusion, this study provides valuable insights into the GNMF models with $\ell_{2,0}$ -norm constraint, presents efficient algorithms for solving them, and demonstrates their effectiveness in clustering and feature selection tasks. Our work contributes to the field of matrix factorization and offers potential for further advancements in data analysis and feature learning.

REFERENCES

- [1] A. Hassani, A. Iranmanesh, and N. Mansouri, "Text mining using nonnegative matrix factorization and latent semantic analysis," *Neural Computing and Applications*, vol. 33, pp. 13 745–13 766, 2021.
- [2] N. Yu, M.-J. Wu, J.-X. Liu, C.-H. Zheng, and Y. Xu, "Correntropy-based hypergraph regularized nmf for clustering and feature selection on multi-cancer integrated data," *IEEE Transactions on Cybernetics*, vol. 51, no. 8, pp. 3952–3963, 2020.
- [3] C.-N. Jiao, Y.-L. Gao, N. Yu, J.-X. Liu, and L.-Y. Qi, "Hypergraph regularized constrained nmf for selecting differentially expressed genes and tumor classification," *IEEE journal of biomedical and health informatics*, vol. 24, no. 10, pp. 3002–3011, 2020.
- [4] C. He, Y. Zheng, X. Fei, H. Li, Z. Hu, and Y. Tang, "Boosting nonnegative matrix factorization based community detection with graph attention auto-encoder," *IEEE Transactions on Big Data*, vol. 8, no. 4, pp. 968–981, 2021.
- [5] H. Gao, F. Nie, and H. Huang, "Local centroids structured non-negative matrix factorization," in *Proceedings of the AAAI Conference on Artificial Intelligence*, vol. 31, no. 1, 2017.
- [6] C. H. Ding, T. Li, and M. I. Jordan, "Convex and semi-nonnegative matrix factorizations," *IEEE Trans. Pattern Anal. Mach. Intell.*, vol. 32, no. 1, pp. 45–55, 2010.
- [7] Y.-X. Wang and Y.-J. Zhang, "Nonnegative matrix factorization: A comprehensive review," *IEEE Trans. Knowl. Data Eng.*, vol. 25, no. 6, pp. 1336–1353, 2013.
- [8] X. Fu, K. Huang, N. D. Sidiropoulos, and W.-K. Ma, "Nonnegative matrix factorization for signal and data analytics: Identifiability, algorithms, and applications," *IEEE Signal Process. Mag.*, vol. 36, no. 2, pp. 59–80, 2019.
- [9] J.-X. Liu, D. Wang, Y.-L. Gao, C.-H. Zheng, Y. Xu, and J. Yu, "Regularized non-negative matrix factorization for identifying differentially expressed genes and clustering samples: a survey," *IEEE/ACM Trans. Comput. Biol. Bioinform.*, vol. 15, no. 3, pp. 974–987, 2017.
- [10] D. Wang, T. Li, P. Deng, J. Liu, W. Huang, and F. Zhang, "A generalized deep learning algorithm based on nmf for multi-

- view clustering,” *IEEE Transactions on Big Data*, vol. 9, no. 1, pp. 328–340, 2022.
- [11] D. Cai, X. He, J. Han, and T. S. Huang, “Graph regularized nonnegative matrix factorization for data representation,” *IEEE transactions on pattern analysis and machine intelligence*, vol. 33, no. 8, pp. 1548–1560, 2010.
- [12] X. Dai, G. Chen, and C. Li, “A discriminant graph nonnegative matrix factorization approach to computer vision,” *Neural Computing and Applications*, vol. 31, pp. 7879–7889, 2019.
- [13] J. Mu, L. Dai, J.-X. Liu, J. Shang, F. Xu, X. Liu, and S. Yuan, “Automatic detection for epileptic seizure using graph-regularized nonnegative matrix factorization and bayesian linear discriminate analysis,” *Biocybernetics and Biomedical Engineering*, vol. 41, no. 4, pp. 1258–1271, 2021.
- [14] X. Xiu, J. Fan, Y. Yang, and W. Liu, “Fault detection using structured joint sparse nonnegative matrix factorization,” *IEEE Transactions on Instrumentation and Measurement*, vol. 70, pp. 1–11, 2021.
- [15] R. Li, G. Yang, K. Wang, Y. Huang, F. Yuan, and Y. Yin, “Robust ecg biometrics using gnmf and sparse representation,” *Pattern Recognition Letters*, vol. 129, pp. 70–76, 2020.
- [16] S. Huang, H. Wang, T. Li, T. Li, and Z. Xu, “Robust graph regularized nonnegative matrix factorization for clustering,” *Data Mining and Knowledge Discovery*, vol. 32, pp. 483–503, 2018.
- [17] R. Zhu, J.-X. Liu, Y.-K. Zhang, and Y. Guo, “A robust manifold graph regularized nonnegative matrix factorization algorithm for cancer gene clustering,” *Molecules*, vol. 22, no. 12, p. 2131, 2017.
- [18] D. Wang, J.-X. Liu, Y.-L. Gao, C.-H. Zheng, and Y. Xu, “Characteristic gene selection based on robust graph regularized non-negative matrix factorization,” *IEEE/ACM transactions on computational biology and bioinformatics*, vol. 13, no. 6, pp. 1059–1067, 2015.
- [19] P. Zhu, W. Zhu, W. Wang, W. Zuo, and Q. Hu, “Non-convex regularized self-representation for unsupervised feature selection,” *Image and Vision Computing*, vol. 60, pp. 22–29, 2017.
- [20] H. Huang, C. Ding, and D. Luo, “Towards structural sparsity: An explicit ℓ_2/ℓ_0 approach,” in *IEEE 10th Int. Conf. Data Mining*, 2010, pp. 344–353.
- [21] T. Pang, F. Nie, J. Han, and X. Li, “Efficient feature selection via $\ell_{2,0}$ -norm constrained sparse regression,” *IEEE Trans. Knowl. Data Eng.*, vol. 31, no. 5, pp. 880–893, 2019.
- [22] X. Du, F. Nie, W. Wang, Y. Yang, and X. Zhou, “Exploiting combination effect for unsupervised feature selection by ℓ_{20} norm,” *IEEE Trans. Neural Netw. Learn. Syst.*, vol. 30, no. 1, pp. 201–214, 2018.
- [23] J. Li, K. Cheng, S. Wang, F. Morstatter, R. P. Trevino, J. Tang, and H. Liu, “Feature selection: A data perspective,” *ACM computing surveys (CSUR)*, vol. 50, no. 6, pp. 1–45, 2017.
- [24] J. Bolte, S. Sabach, and M. Teboulle, “Proximal alternating linearized minimization for nonconvex and nonsmooth problems,” *Math. Program.*, vol. 146, no. 1-2, pp. 459–494, 2014.
- [25] J. Fan, M. Zhao, and T. W. Chow, “Matrix completion via sparse factorization solved by accelerated proximal alternating linearized minimization,” *IEEE Transactions on Big Data*, vol. 6, no. 1, pp. 119–130, 2018.
- [26] T. Pock and S. Sabach, “Inertial proximal alternating linearized minimization (ipalm) for nonconvex and nonsmooth problems,” *SIAM journal on imaging sciences*, vol. 9, no. 4, pp. 1756–1787, 2016.
- [27] Y. Xu and W. Yin, “A globally convergent algorithm for nonconvex optimization based on block coordinate update,” *Journal of Scientific Computing*, vol. 72, no. 2, pp. 700–734, 2017.
- [28] D. D. Lee and H. S. Seung, “Learning the parts of objects by non-negative matrix factorization,” *Nature*, vol. 401, no. 6755, pp. 788–791, 1999.
- [29] K. Chen, H. Che, X. Li, and M.-F. Leung, “Graph non-negative matrix factorization with alternative smoothed l_0 regularizations,” *Neural Computing and Applications*, vol. 35, no. 14, pp. 9995–10009, 2023.
- [30] W. Min, T. Xu, X. Wan, and T.-H. Chang, “Structured sparse non-negative matrix factorization with $\ell_{2,0}$ -norm,” *IEEE Transactions on Knowledge and Data Engineering*, 2022.
- [31] N. Guan, D. Tao, Z. Luo, and B. Yuan, “NeNMF: An optimal gradient method for nonnegative matrix factorization,” *IEEE Trans. Signal Process.*, vol. 60, no. 6, pp. 2882–2898, 2012.
- [32] W. Yang and W. Min, “An accelerated block proximal framework with adaptive momentum for nonconvex and nonsmooth optimization,” *arXiv preprint arXiv:2308.12126*, 2023.
- [33] X. Yang and L. Xu, “Some accelerated alternating proximal gradient algorithms for a class of nonconvex nonsmooth problems,” *Journal of Global Optimization*, pp. 1–26, 2022.
- [34] Q. Li, Y. Zhou, Y. Liang, and P. K. Varshney, “Convergence analysis of proximal gradient with momentum for nonconvex optimization,” in *Int. Conf. Mach. Learn.*, 2017, pp. 2111–2119.
- [35] X. Chang, Y. Wang, R. Li, and Z. Xu, “Sparse k-means with ℓ_∞/ℓ_0 penalty for high-dimensional data clustering,” *Stat. Sin.*, vol. 28, no. 3, pp. 1265–1284, 2018.
- [36] Z. Li, J. Liu, Y. Yang, X. Zhou, and H. Lu, “Clustering-guided sparse structural learning for unsupervised feature selection,” *IEEE Trans. Knowl. Data Eng.*, vol. 26, no. 9, pp. 2138–2150, 2014.
- [37] D. Dua, C. Graff *et al.*, “Uci machine learning repository,” 2017.
- [38] L. Van der Maaten and G. Hinton, “Visualizing data using t-sne.” *Journal of machine learning research*, vol. 9, no. 11, 2008.



China, from 2019 to 2021.

His current research interests include machine/deep learning, sparse optimization and bioinformatics. He has authored about 30 papers in journals and conferences, such as the IEEE Trans Knowl Data Eng, IEEE Trans Image Process, IEEE Trans Neural Netw Learn Syst, PLoS Comput Biol, Bioinformatics, IEEE/ACM Trans Comput Biol Bioinform, and IEEE International Conference on Bioinformatics and Biomedicine.



Zhen Wang is currently pursuing a master's degree at the School of Information Science and Engineering, Yunnan University.

His current research interests include machine/deep learning, sparse optimization and graph machine learning.